2021 IEEE 12th Annual Ubiquitous Computing, Electronics & Mobile Communication Conference (UEMCON) | 978-1-6654-0690-1/21/$31.00 ©2021 IEEE | DOI: 10.1109/UEMCON53757.2021.9666498

Atmospheric Turbulence Identification in a multi-user FSOC using Supervised Machine Learning

Federica Aveta
School of Electrical and Computer Engineering
Wentworth Institute of Technology
Boston, MA, USA
avetaf@wit.edu

Samuel Chan, Nabil Asfari, Hazem Refai
Department of Electrical and omputer Engineering
Oklahoma University
Tulsa, OK, USA
samuelchan@ou.edu, asfari@ou.edu, hazem@ou.edu

***Abstract*— Atmospheric turbulence can heavily affect free space optical communication (FSOC) link reliability. This introduces random fluctuations of the received signal intensity, resulting in degraded system communication performance. While extensive research has been conducted to estimate atmospheric turbulence on single user FSOC, the effects of turbulent channel on multi-point FSOC has recently gained attention. In fact, latest results showed the feasibility of multi-user FSOC when users, sharing time and bandwidth resources, communicate with a single optical access node. This paper presents a machine learning (ML)-based methodology to identify how many users are concurrently transmitting and overlapping into a single receiver interfering within each other, and which one is propagating through a turbulent channel. The proposed methodology presents two different approaches based on: 1) traditional classification ML algorithms and 2) Convolutional Neural Network (CNN). Both methods employ amplitude distribution of the received mixed signals as input features. 100% validation accuracy was achieved by CNN employing an experimental data set of 900 images.**

Keywords—Free Space Optical Communication (FSOC), multi-user, atmospheric turbulence, Machine Learning (ML), Convolutional Neural Network (CNN).

I. INTRODUCTION

The increasing demand for more spectral bandwidth by the military, government, and commercial wireless industries are leading to explore the use of new wireless solutions to overcome the challenges of radio frequency (RF) spectrum-scarce environment [1]. Free space optical communication (FSOC) systems have gained an increasing interest as promising technology for potentially overcoming RF spectrum scarcity. Advantages over traditional RF communication include higher bandwidth and higher capacity; sizeable, license-free spectrum; quick and easy deployment; reduced power, cost and size; and better security [2], [3]. However, given its narrow light beam-width, free-space optics (FSO) is inherently a point-to-point communication technology whose state-of-the-art available systems do not support multiple-user communication. Moreover, FSO technology is heavily degraded by atmospheric perturbations. These random changes in the refractive index are due to inhomogeneities in the temperature and the pressure of the atmosphere. This causes random variations in the amplitude and phase of the optical wave propagating in the turbulent medium, resulting in a degraded optical signal (i.e., channel fading) [2]. Therefore, fluctuation of the received signal intensity (scintillations) affects the performance quality of the optical wireless communication system reducing the bit error rate (BER) [4]. Recent studies investigated various techniques to quantitatively estimate atmospheric turbulence. Proposed methodologies mainly consider: 1) Channel State Information (CSI) methods, where pilot signals were sent to detect the channel condition [5], 2) blind detection methods that did not use pilot signals decreasing the information quality, while increasing the throughput [6], [7] and 3) machine learning (ML) -based regression and classification methodologies [8]–[10].

All methodologies focused on atmospheric turbulence estimation for a single-user FSOC. However, recent studies successfully demonstrated multi-point FSOC, where multiple users, sharing resource allocation (time, bandwidth and space), concurrently transmit into a single node optical receivers [11], [12]. As such, transmitted signals overlap at receiver side causing users interference, making estimation of turbulence effects on single user a challenging task. In this paper, we propose a methodology to automatically identify the number of concurrently transmitting users, and which users propagates through a turbulent channel, without any interference mitigation. Two different classification approaches based on 1) traditional ML and 2) CNN employing the received mixed signal amplitude were tested. Experimental validation was conducted on a setup comprised of three users and an atmospheric turbulence box to generate a turbulent channel.

II. EXPERIMENTAL SETUP

A. Experimental Setup

Fig. 1 shows a picture of the complete experimental setups. The setup consists of three users based on an intensity modulation with direct detection (IM/DD) scheme. User 1 consisted of high-speed digital reference optical transmitter (C-band), namely Thorlabs MX10B, driven by a pseudo-random bit sequence (PRBS) with 2^5–1 bit in length and 200 Mbps data rate. Users 2 and 3 consisted of two optical module transceivers (SFP) (1310 nm) independently driven, via Hitech Global SMA

978-1-6654-0690-1/21/$31.00 ©2021 IEEE

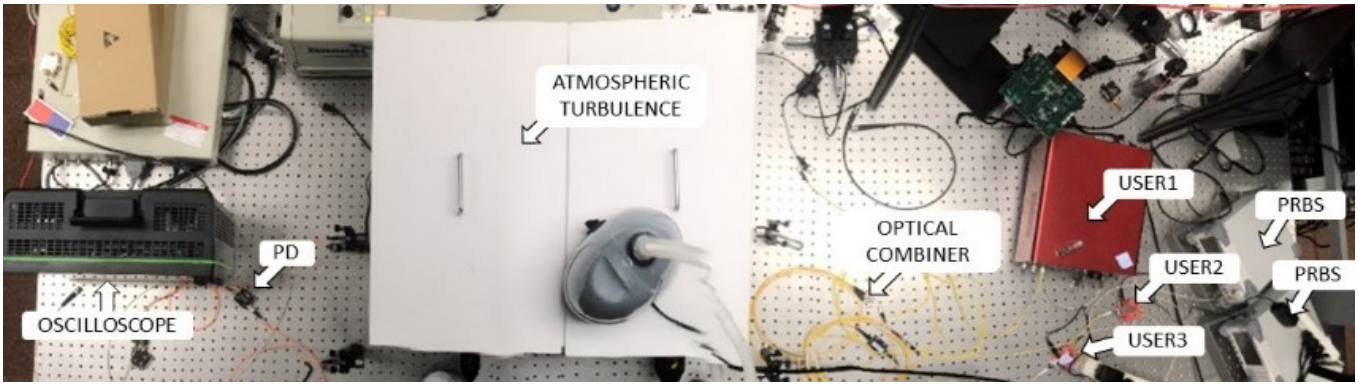

Fig. 1: Picture of the experimental setup

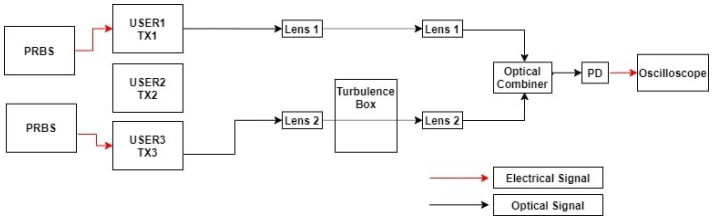

Fig. 2: Block diagram for Class 2

to SFP Conversion Module, by PRBSs with 2^7–1 and 2^9–1 bit in length respectively, and 200 Mbps data rate. PRBSs were generated through dual-channel Pulse/Arbitrary Waveform Generators, namely SIGLENT's SDG6032X. Transmitted powers were set with a 2 dB power difference as follow: TX_{user1} = 1.29 dBm, TX_{user2} = -1.48 dBm, TX_{user3} = -3.80 dBm. Transmitted signals were combined with the usage of several optical combiners (e.g., 4x1, 2x1, 2x2, etc.,) to cover the nine users' combinations, described in Table I. Two pairs of collimators with 1550-nm wavelength-dependent and 1310-nm wavelength-dependent lenses were used to propagate the combined signals through the free space turbulent and/or non-turbulent channel. To emulate the turbulent channel, a turbulence box equipped with heating elements on the bottom, four AC fans, two variable humidifiers, and a ventilation aperture was used. Turbulence was set at temperature of 58.61 °C, wind speed of 14.21 m/s, and relative humidity of 80.56% [12]. The box was placed between the collimators pair to generate turbulent channel. The received optical signal was collected by 5-GHz InGaAs photodetector, namely Thorlabs DET08CFC.

B. Data Collection

Data was collected using oscilloscope with 20 GSample/s sampling rate. Each acquisition consisted of 5,000 samples, and continuous collection was held until roughly 5,000 acquisitions were collected for each scenario. Each file was then saved as a 1x5000 vector (.dat) by the built-in interface of WavePro 254HD-MS and was transferred to a PC via ethernet for postprocessing. Fig. 2 shows the block diagram of the setup used for data collection for scenario 2 (See Table I) with two users, only one affected by turbulence. The red connections represent the electrical links, the black continuous lines represent the fiber optical links, and the black dashed lines represent the free-space optical links. Users 1 and user 2 were set as described in section II.A. User 1 propagated through the free-space non-turbulent channel, and user 2 through the free-space turbulent channel. Propagation occurred with two collimators pairs (called as Lens1 and 2 in the diagram). Received signals were mixed (using the optical combiner) and collected by a single photodiode, then sent into the oscilloscope. By different configurations of the optical combiners, all the scenarios listed in Table I were generated.

III. Methodology

A. Pre-processing

FSOC link can be significantly affected by atmospheric turbulence-induced scintillation, which leads to power loss, random fluctuation of the received intensity, and degraded communication performance. As such, empirical histogram of received mixed signal amplitude is sensitive to power fluctuations. Fig. 3 a) and b) show the received mixed signals with two simultaneously transmitting users without turbulence and two users with turbulence. Whereas, Fig. 3 c) and d) show the corresponding amplitude distribution. Note that, turbulent channel effects on the histograms lead to peaks broadening (peaks width) and attenuation (peaks location). Therefore, histograms of the received signals amplitude were used as input feature for our study.

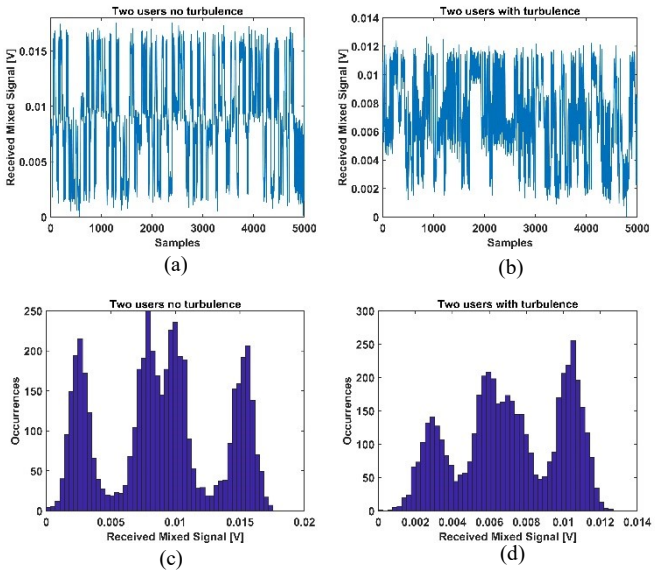

Fig. 3: Received mixed signal without turbulence (a) and with turbulence (b); histogram of signal in a (c) and in b (d).

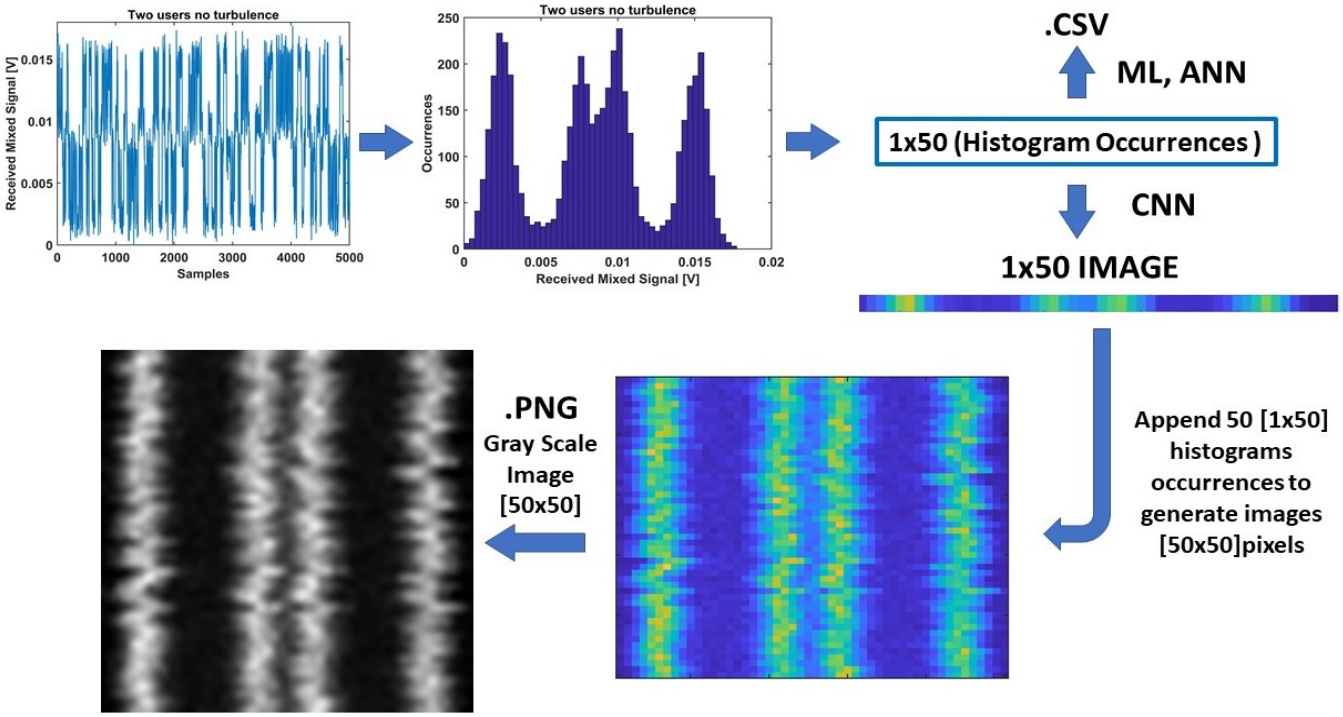

Fig. 4: Data Pre-Processing

Data pre-processing was performed to make the data format suitable for the two approaches that were employed: traditional ML classifiers (k-NN, SVM, Ensemble, ANN) and DNN (CNN) classifier. Data preparation steps are illustrated in Fig. 4 for two users without turbulence. For each scenario (See Table I) the time series received mixed signal was saved. Each acquisition consists of 5,000 samples that correspond to an acquisition time of $T = 0.25\ \mu s$ such that, $T \ll T_C$ (T_C is the atmospheric turbulence coherence time [$\sim ms$]) [13]. Then, the distribution of the received signal amplitude was computed, resulting in the empirical histogram realized with 50 bins. Occurrence values are extracted from the histogram and stored in a .csv file for the traditional ML analysis. The same procedure was used for all the acquisitions and scenarios resulting in a .csv file with 45,400 rows (instances). For the DNN analysis, the extracted occurrence values were saved as 1x50 pixels image. Then the same procedure was conducted for other acquisitions, and 50 [1x50] images were appended to generate a 50x50 pixels images. The final images showed the number of bins on the x-axes, the number of analyzed acquisitions/histograms (that correspond to an acquisition time $T = 12.5\ \mu s \ll T_C$) on the y-axis, and the histogram occurrences values on the z-axis. Obtained images were transformed into grayscale images (.png) for input into the CNN model, to reduce computation complexity. The data set consisted of 908 images (~100 per scenario). Fig 5 shows examples of generated images for two users (a) one affected by turbulence, and (b) both affected by turbulence. Outputs for both classification methodologies consist in nine classes that correspond to the tested scenarios and are encoded as illustrated in Table I.

Table I: Class Encoding

SCENARIO	CLASS
Two users no turbulence	**1**
Two users one with turbulence	**2**
Two users all with turbulence	**3**
Three users no turbulence	**4**
Three users one with turbulence	**5**
Three users two with turbulence	**6**
Three users all with turbulence	**7**
One user no turbulence	**8**
One user with turbulence	**9**

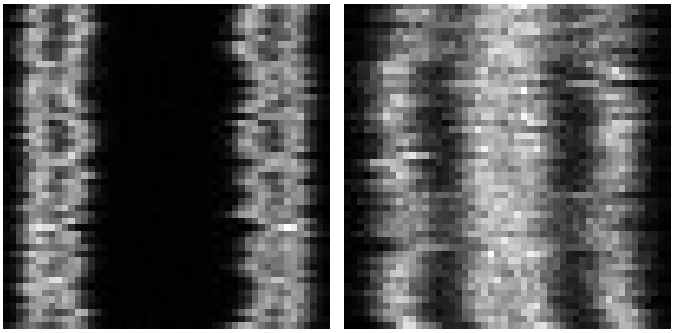

(a) (b)

Fig. 5: Images for two users: (a) one with turbulence; (b) both with turbulence

Comparing Fig. 5 with the image in Fig. 4, it is clear how the turbulence affects the amplitude distribution introducing attenuation and fluctuation on the received signals. As such, histogram peaks are subject to random shift of their location, for example in Fig. 5 (b) the two peaks in the middle almost merge making it difficult to identify them separately.

B. Machine Learning Classifiers

Various machine learning classification algorithms are investigated for their performance comparison. A brief overview and insights from each of these algorithms are also provided [14].

- **K-NN:** Supervised learning. K-point of classified neighbor samples determine an unclassified sample object by plurality vote. The object is being assigned to a most common class among its K-nearest neighbors.
- **SVM:** Supervised learning. SVM calculates the best hyperplanes that have maximum margins from two or more classes, decision boundaries were created to classify different labels.
- **Ensemble:** Better prediction could be obtained by using ensemble methods by having multiple learning algorithms than that could be obtained from any single learning algorithm alone [15].
- **Decision Tree:** Supervised learning. Decision Tree has a flow-chart like structure, it predicts by calculating target value from observations of branches, each branch represents an outcome from a test on an attribute. Information gain could be used to calculate its target value.
- **ANN:** Supervised or unsupervised learning. A class of deep neural networks that contains multi-layers. ANNs are forms of artificial neurons which hold the concept of neurons from biological brains, which process and combine input with their internal state, and an optional threshold using an activation function. The connections of the neurons, weighting assigning, and output functions produce an output, mostly an outcome of a probability. Classification could be done by passing data into the network, parameter of the network would be learnt and adjusted to make prediction [16].
- **CNN:** Supervised or unsupervised learning. A class of deep neural networks that contains multi-layers. Block-building-like structure is mostly used to represent the architecture of the network. CNN learns the filters (kernels) which are used to extract features from input using convolution operation [17]. Other techniques often apply for handling massive amount of input, such as pooling layer, max pooling, and RELU layer. CNN is often used for image classification due to the learning of filters.

IV. Results

We evaluated the effectiveness of each classification model using primarily two metrics: classification accuracy, and training time. Then, the obtained results were used to compare the tested algorithms to choose the best available model. The hold-out validation method was employed for the analysis with 90% of the data for training and 10% for testing. This section details the model parameters selected for the analysis and the model's classification performance.

A. ML Classifiers

K-NN, SVM, Bagged Tree and Decision Tree model parameters and results are reported here. K-NN was set with K=1 and Euclidean distance as similarity metric. A linear kernel was selected for SVM. Bagged Tree was run with 50 maximum number of splits and 30 learners; and decision tree was set with 100 maximum number of splits, and Gini index as purity measure. All models were trained and tested five different times. Testing accuracy and training time were recorded for each case. Fig. 6 shows the average testing accuracy [%] within its standard deviation (error bars): (a) average training time [s] (b) versus the tested algorithms. All classifiers were able to accurately classify the number of communicating users affected by turbulence. Accuracy greater than 94% was achieved with all methodologies, and the highest accuracy of 98.36% for bagged tree.

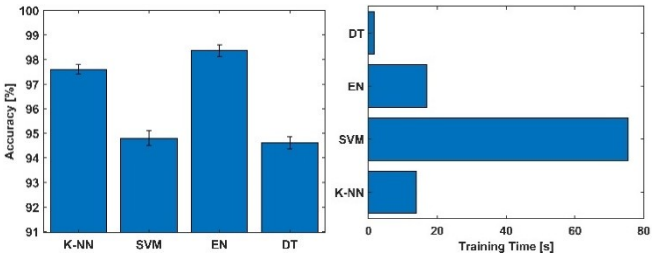

Fig. 6: Accuracy (a) and training time (b) versus classifier model

To identify the configurations that most contribute to the error defined as: $error = 1 - accuracy$, a confusion matrix for SVM model illustrating prediction error per class is shown in Fig. 7. The green boxes on the right represent the true positive rate (TPR), while the red boxes represent the false negative rate (FNR). One user with turbulence was found to be the main culprit for misclassification error. This was evident in the confusion matrix where high FNR=0.24 and low TPR=0.76 was measured. Histogram of the received single user amplitude has two peaks (two overlapping users show four peaks, and three users eight peaks) [11]. Therefore, the results suggest that the interaction between users and peaks separation contain useful information for accurate classification.

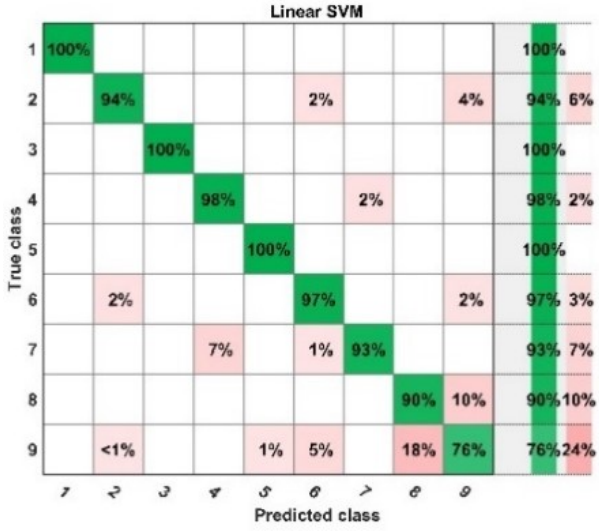

Fig. 7: SVM confusion matrix

B. *Artificial Neural Network*

The ANN was built using 45,000 inputs (number of instances), one hidden layer and 9 outputs (number of classes). The network was trained using the *scaled conjugate gradient backpropagation* algorithm and cross-entropy was selected as loss function. The optimum number of neurons n in the ANN hidden layer to maximize classification performance was investigated. ANN model was trained and tested five different times, and testing accuracy and training time were recorded for each case. Fig. 8 shows (a) the average accuracy and its standard deviation, and (b) the training time [s] versus the tested number of neurons n =[1:1:40].

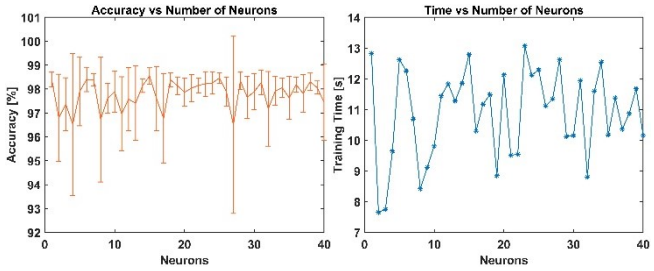

Fig. 8: ANN accuracy (a) and training time (b) versus number of neurons

Results show that the trained model guarantees high classification accuracy (>96%) for all the range of tested neurons. Maximum average accuracy of 98.54% (0.34% standard deviation) was achieved with 15 neurons and a training time of 12.92 [s]. $n = 15$ was selected for further algorithms comparison detailed in Section IV.D.

C. *Convolutional Neural Network*

A CNN architecture was developed to train and classify generated images from the histogram amplitude of the received mixed signals, as shown in Fig. 5. An initial learning rate of 0.01 was selected, the maximum number of epochs was initially set to 7, and the batch size to 128. The CNN structure consists of 2 transformation layers, followed by one dense fully connected layer. Table II describes each layer in the CNN network architecture in detail.

Table II: CNN parameters

Layer Name	Activations	Filters/Pooling Size	Filter Stride
Image Input	50x50x1	-	
Convolution	50x226x8	3 x 3 x 1	1
Batch Normalization	50x50x8	-	-
ReLU	50x50x8	-	-
Max Pooling	25x25x8	2 x 2	2
Convolution	25x25x16	3 x 3 x 8	1
Batch Normalization	25x25x16	-	-
ReLU	25x25x16	-	-
Max Pooling	12x12x16	2 x 2	2
Fully Connected	1x1x9	-	-
Softmax	1x1x9	-	-
Classification Output	-	-	-

The 2-D convolutional layer applies sliding convolutional filters with a given filter size and step (stride) to the input images. The batch normalization layer normalizes each input channel, speeding up the training of convolutional neural networks. A ReLU is a nonlinear activation function that performs a threshold operation to each element of the input, where any value less than zero, is set to zero. The max pooling layer performs down-sampling by dividing the input into rectangular pooling regions and computing the maximum of each region. The fully connected layer combines all of the features learned by the previous layers across the image, to classify the images. Fig. 9 shows the validation (black dashed line) and training (blue line) accuracy versus the number of iterations and epochs. 100% training and validation accuracy was achieved at 3rd epoch with a training time of 9[s]. CNN model was trained and tested five times and maximum accuracy was achieved for each run.

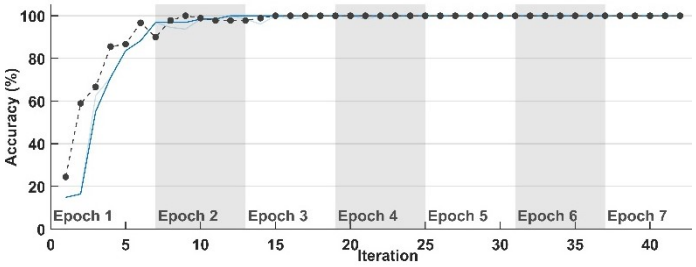

Fig. 9: CNN accuracy

D. *Discussion*

The results attained from the previous analysis are compared to evaluate models in terms of achieved accuracy and required training time, as illustrated in Fig. 10.

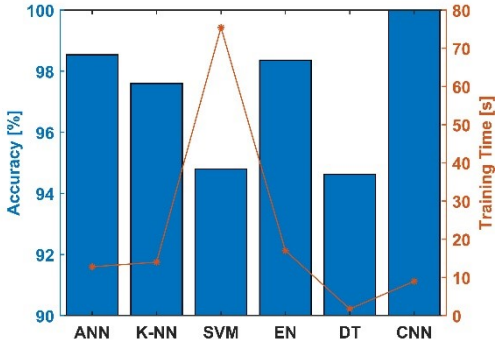

Fig. 10: Models comparison

Note that the proposed CNN model outperformed the other classification models achieving 100% validation accuracy with low-training time (9[s]). In fact, CNN is capable of automatically detecting and extracting *high-level features* from input images to correctly classify them.

V. Conclusion

Atmospheric turbulence worsens FSOC link reliability, degrading the received signal quality. In this work, we propose a ML-based method to identify atmospheric turbulence effects on a single user when multiple users, sharing allocation resources, communicate into a single node optical receiver, interfering within each other. The methodology uses histogram of the received mixed signals amplitude as input features.

Several algorithms were experimentally validated: traditional ML classifiers (SVM, K-NN, ANN, Ensemble and Decision Tree) and Convolutional Neural Network (CNN). Results demonstrated high classification accuracy. CNN outperformed the other classifiers achieving 100% validation accuracy and low training time 9[s].

Future work will focus on quantitatively measuring turbulence-induced scintillations for each user undergoing turbulent channel. Regression analysis will be used to estimate the refractive index structure parameter C_n^2 for each channel turbulence.

REFERENCES

[1] G. Staple and K. Werbach, "The end of spectrum scarcity [spectrum allocation and utilization]," *IEEE Spectr.*, vol. 41, no. 3, pp. 48–52, 2004.

[2] H. Kaushal and G. Kaddoum, "Optical communication in space: Challenges and mitigation techniques," *IEEE Commun. Surv. Tutorials*, vol. 19, no. 1, pp. 57–96, 2017.

[3] M. A. Khalighi and M. Uysal, "Survey on Free Space Optical Communication: A Communication Theory Perspective," *IEEE Commun. Surv. Tutorials*, vol. 16, no. 4, pp. 2231–2258, 2014.

[4] M. Uysal, C. Capsoni, Z. Ghassemlooy, A. Boucouvalas, and E. Udvary, *Optical wireless communications: an emerging technology*. Springer, 2016.

[5] V. Srivastava and M. Motani, "Cross-layer design: a survey and the road ahead," *IEEE Commun. Mag.*, vol. 43, no. 12, pp. 112–119, 2005.

[6] M. T. Dabiri, S. M. S. Sadough, and H. Safi, "Closed-form error probability of blind detection for free space optical systems," in *2016 8th International Symposium on Telecommunications (IST)*, 2016, pp. 304–308.

[7] M. Elbawab, M. Abaza, and M. H Aly, "Blind Detection for Serial Relays in Free Space Optical Communication Systems," *Appl. Sci.*, vol. 8, no. 11, p. 2074, 2018.

[8] J. J. Rudiger, K. Book, J. S. deGrassie, S. Hammel, and B. Baker, "A machine learning approach for forecasting the refractive index structure parameter," in *Laser Communication and Propagation through the Atmosphere and Oceans VII*, 2018, vol. 10770, p. 107700P.

[9] M. A. Amirabadi, M. H. Kahaei, S. A. Nezamalhosseini, and V. T. Vakili, "Deep Learning for channel estimation in FSO communication system," *Opt. Commun.*, vol. 459, p. 124989, 2020.

[10] Y. Wang and S. Basu, "Estimation of optical turbulence in the atmospheric surface layer from routine meteorological observations: an artificial neural network approach," in *Laser Communication and Propagation through the Atmosphere and Oceans III*, 2014, vol. 9224, p. 92240X.

[11] F. Aveta, H. H. Refai, and P. G. LoPresti, "Number of Users Detection in Multi-Point FSOC Using Unsupervised Machine Learning," *IEEE Photonics Technol. Lett. [In Press.*, 2019.

[12] F. Aveta, H. H. Refai, and P. LoPresti, "Multiple access technique in a high-speed free-space optical communication link: independent component analysis," *Opt. Eng.*, vol. 58, no. 3, p. 36111, 2019.

[13] I. E. Lee, Z. Ghassemlooy, W. P. Ng, and M. Uysal, "Performance analysis of free space optical links over turbulence and misalignment induced fading channels," in *Communication Systems, Networks & Digital Signal Processing (CSNDSP), 2012 8th International Symposium on*, 2012, pp. 1–6.

[14] P.-N. Tan, M. Steinbach, and V. Kumar, *Introduction to data mining*. Pearson Education India, 2016.

[15] D. Opitz and R. Maclin, "Popular ensemble methods: An empirical study," *J. Artif. Intell. Res.*, vol. 11, pp. 169–198, 1999.

[16] J. Schmidhuber, "Deep learning in neural networks: An overview," *Neural networks*, vol. 61, pp. 85–117, 2015.

[17] D. C. Ciresan, U. Meier, J. Masci, L. M. Gambardella, and J. Schmidhuber, "Flexible, high performance convolutional neural networks for image classification," in *Twenty-Second International Joint Conference on Artificial Intelligence*, 2011.